Journal of the Korean Data & Information Science Society
2021, **32**(2), 427–437

http://dx.doi.org/10.7465/jkdi.2021.32.2.427
한국데이터정보과학회지

Confusion plot for the confusion matrix

Chong Sun Hong[1]

[1]Department of Statistics, Sungkyunkwan University

Received 8 December 2020, revised 28 January 2021, accepted 8 February 2021

Abstract

There is a well known 2 by 2 confusion matrix which is widely used in biostatistics or credit assessment. Using these, not only the true positive rate (TPR) and true negative rate (TNR) but also the positive predictive value (PPV) and negative predictive value (NPV) statistics are obtained. In this study, we propose the confusion plot which is a graphical method can geometrically describe various statistics defined from the confusion matrix. The confusion plot consists of six right-angled triangles using equations expressed as the sum of rows and columns of the confusion matrix. In particular, it is found that TPR, TNR, PPV and NPV can be described as acute angles of right-angled triangles in the confusion plot. This confusion plot can evaluate the classification model and its performance similarly to the well known ROC curve. Therefore, the confusion plot could be useful in evaluating the classification models similar to the ROC curve.

Keywords: Confusion matrix, NPV, PPV, TNR, TPR.

1. Introduction

Statistical classification results can be expressed by the confusion matrix shown in Table 1 for various areas such as biostatistics and credit evaluation. Let the set C represent the patient states and be assumed to consist of two elements, $C = \{0,\ 1\}$, where element 0 and 1 represent non-disease/non-default/negative and disease/default/positive states, respectively. The TP (true positive) and TN (true negative) in Table 1.1 represent the number of correctly classified disease and normal populations, respectively. In other words, the TP is the number of patient with an actual disease will be positive ($\hat{C} = 1$) and the TN is the number of normal person to be negative ($\hat{C} = 0$). But the FP (false positive) and FN (false negative) are numbers of groups that predicted disease as normal and predicted normal as disease, respectively. The total number of disease groups, p, is TP+FN in the population, and the number of normal populations, q, is FP+TN. And assume that both p and q are known (Metz and Kronman, 1980; Swets, 1988; Hsieh *et al.*, 1996; Provost and Fawcett, 1997; Engelmann *et al.*, 2003; Pepe *et al.*, 2003; Fawcett, 2004, 2006; Stein, 2005; Sonego *et al.*, 2008; Hong *et al.*, 2010; Hong and Wu, 2014; Cho and Hong, 2015; Hong *et al.*, 2019a,b).

[1] Professor, Department of Statistics, Sungkyunkwan University, 25-2, Sungkyunkwan-Ro, Jongno-Gu, Seoul 03063, Korea. E-mail: cshong@skku.edu

Table 1.1 Confusion matrix

		$\hat{C}$		Sum
		1	0	
C	1	TP	FN	p
	0	FP	TN	q
Sum		$\hat{p}$	$\hat{q}$	N

The TPR and TNR are expressed by the following probability equations:

$$TPR = P(\hat{C} = 1|C = 1) = TP/(TP + FN),$$
$$TNR = P(\hat{C} = 0|C = 0) = TN/(TN + FP).$$

Note that the TPR and TNR are also known as the sensitivity and specificity, respectively (Altman and Bland,1994).

When the evaluation result of the disease is positive or negative, one may want to know the probability of the test performance that an actual health condition is disease or normal rather than how accurate the diagnosis is. Hence, there are two probability measures: the PPV (positive predictive value) and NPV (negative predictive value) suggested by Raslich *et al.* (2007) and Zhou *et al.* (2002). The probability that the patient determined to have the disease is actually a disease is called the PPV, and the probability that the determined patient is actually normal is called the NPV. Also, the PPV tells the clinician what percent of those with a positive finding has the disease, and the NPV reveals what percent of those with a negative result do not have the disease. Both the PPV and NPV can be expressed as (Shiu and Gatsonis, 2008; Zhou *et al.*, 2009; Jeske, 2018; Hughes, 2020; Oehr and Ecke, 2020):

$$PPV = P(C = 1|\hat{C} = 1) = TP/(TP + FP),$$
$$NPV = P(C = 0|\hat{C} = 0) = TN/(TN + FN).$$

Based on statistical decision theory, the ROC (receiver operating characteristic) curve is a visual tool that can easily identify the classifier's performance in binary classification (Green and Swets, 1966; Bamber, 1975; Egan and Egan, 1975; Hanley and McNeil, 1982; Swets, 1988; Centor, 1991; Zweig and Campbell, 1993; Fawcett, 2004; Vuk and Curk, 2006; Tasche, 2008). Since the ROC curve is implemented with (1-TNR, TPR) in a unit length square, the TPR and TNR can be represented on the ROC curve. In contrast, the PPV and NPV cannot be explored in the ROC curve. Pontius and Si (2014) proposed the TOC (total operating characteristic) curve which is implemented in a parallelogram with a hypotenuse slope of 45 degrees (Hong and Choi, 2020; Hong and Lee, 2018). Hong and Choi (2020) showed that the PPV and NPV are explained on the TOC curve in terms of geometry.

In this work, a graphical method is proposed to describe geometrically various statistics such as the TPR and TNR as well as the PPV and NPV which are defined as ratios based on the confusion matrix. This geometrical representation is consisted with several right-angled triangles. Each right-angled triangle is based on a sum equation of the row or column of the confusion matrix. It could show that a certain angle of a right-angled triangle is described a ratio based on the confusion matrix.

Section 2 of this paper suggests the TPR - TNR plot which can describe the TPR and TNR as well as the FPR (=1-TPR) and FNR (=1-TNR) geometrically. Moreover, the PPV - NPV

Table 2.1 An example of confusion matrix

		$\hat{C}$		Sum
		1	0	
C	1	90	10	100
	0	30	120	150
Sum		120	130	

plot is also proposed to explain the PPV and NPV geometrically. These TPR, TNR, PPV and NPV are shown to define as functions of corresponding angles of right-angled triangles. Both the TPR - TNR and PPV - NPV plots have common line segments, so that these two plots can be put together into one. This combined plot of the TPR - TNR and PPV - NPV plots is developed in Section 3. This is called as the confusion plot. With the confusion plot, the TPR, TNR, PPV and NPV are described geometrically as functions of corresponding angles of right-angled triangles. The FPR and FNR are also explained as well as the total probability of disease based on the confusion plot. In Section 4, various shaped confusion plots corresponding to several confusion matrices are explored and discussed. Two normal distribution functions are considered in Section 5. Based on a certain threshold for the two distribution functions, a confusion matrix could be obtained. Then, with the confusion matrix, a confusion plot can be drawn. Using this procedure, various confusion plots are compared. Therefore, some meaningful results could be summarized. An empirical data is illustrated and explained using a confusion plot based on the confusion matrix determined by an optimal threshold in Section 6. The final Section 7 summarizes conclusions of this work.

2. TPR - TNR plot and PPV - NPV plot

With an equation $A+B=C$, one can draw a right-angled triangle with three line segments of lengths $\sqrt{A}$, $\sqrt{B}$ and $\sqrt{C}$ using the Pythagorean theorem. From the confusion matrix in Table 1.1, the following three equations are obtained

$$\begin{aligned} p+\ q &= N, \\ TP+\ FN &= p, \\ FP+\ TN &= q. \end{aligned} \tag{2.1}$$

Three right-angled triangles can be implemented from three equations in (2.1). The first and second equations in (2.1) have a common p, and the first and third equations have a common q. Hence, three right-angled triangles could be combine together into one plot like Figure 2.1(a). This plot is based on an example in Table 2.1.

From Figure 2.1(a), the length of the horizontal line is $\sqrt{N}$, and the leftmost and rightmost segments are represented by $\sqrt{TP}$ and $\sqrt{TN}$, respectively. Therefore, the TPR and TNR can be explained in Remark 1.

Remark 1: The TPR and TNR are defined by the following equations:

$$TPR\ =\ \cos^2\theta_1,\ \ TNR\ =\ \cos^2\theta_2.$$

□

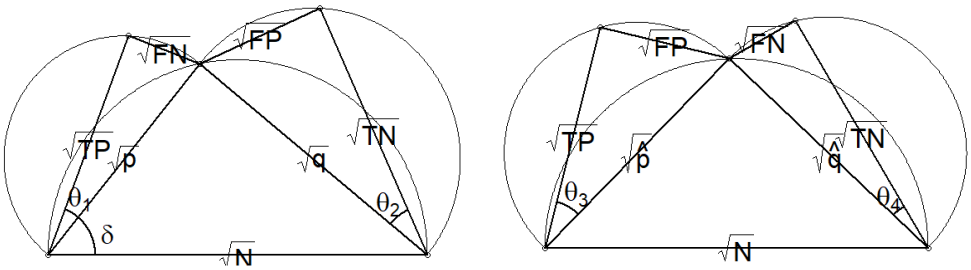

Figure 2.1 TPR - TNR plot and PPV - NPV plot

Note that $\theta_1 = \cos^{-1}\sqrt{TPR}$, $\theta_2 = \cos^{-1}\sqrt{TNR}$. Therefore, the TPR and TNR are described by two acute angles θ_1 and θ_2 in Figure 1(a). If two angles θ_1 and θ_2 are close to zero, then we can interpret that the TPR and TNR have very large ratios. We call this plot as the TPR - TNR plot. Moreover, one can derive that $FPR = \cos^2(\pi/2 - \theta_1)$ and $FNR = \cos^2(\pi/2 - \theta_2)$ as well as $\cos^2\delta = p/(p+q)$, which is used to defined as the total probability of disease.

From Table 2.1 and Figure 2.1(a), one obtains that $TPR = 0.9000$, $TNR = 0.8000$, $\theta_1 = 18.4349°$, $\theta_2 = 26.5651°$ and $\delta = 50.7685°$. Since both the TPR and TNR have large values, two angles of θ_1 and θ_2 are similar and have small degrees.

From the confusion matrix in Table 1.1, another three equations are also obtained:

$$\begin{aligned} \hat{p} + \hat{q} &= N, \\ TP + FP &= \hat{p}, \\ FN + TN &= \hat{q}. \end{aligned} \tag{2.2}$$

Three right-angled triangles are also drawn with three equations in (2.2). With similar arguments, these three right-angled triangles could be represented together as shown in Figure 2.1(b), since the first and second equations in (2.2) have a common $\hat{p}$, and the first and third equations have a common $\hat{q}$. The lengths of the leftmost, rightmost and horizontal line segments in Figure 2.1(b) are represented $\sqrt{TP}$, $\sqrt{TN}$ and $\sqrt{N}$, respectively. These three lines are the same meaning as in Figure 2.1(a). However, using Figure 2.1(b), the PPV and NPV can be described in Remark 2.

Remark 2: The PPV and NPV are explained geometrically by the following equations:

$$PPV = \cos^2\theta_3, \quad NPV = \cos^2\theta_4.$$

□

Note that $\theta_3 = \cos^{-1}\sqrt{PPV}$, $\theta_4 = \cos^{-1}\sqrt{NPV}$. Therefore, the PPV and NPV are described with two acute angles θ_3 and θ_4 in Figure 1(b). If both angles θ_3 and θ_4 are close to 90 degrees ($\pi/2$), then the PPV and NPV have very small values. We call this plot as the PPV - NPV plot.

Figure 2.1(b) is also based on an example in Table 2.1. From Table 2.1 and Figure 2.1(b), one obtains that $PPV = 0.7500$, $NPV = 0.9291$, $\theta_3 = 30.0000°$ and $\theta_4 = 16.1021°$. Since both TPR and NPV have large values, two angles of θ_1 and θ_4 have similar small degrees. Hence, it is found that the PPV - NPV plot has different shape from the TPR - TNR plot.

3. Confusion plot

The TPR - TNR and PPV - NPV plots in Figure 2.1(a,b) have the same horizontal line whose length is $\sqrt{N}$. Moreover, the leftmost and rightmost line segments in Figure 2.1(a,b) represent the equivalent $\sqrt{TP}$ and $\sqrt{TN}$, respectively. Hence, the TPR - TNR plot and the PPV - NPV plot could be combined into one as shown in Figure 3.1. The above part of Figure 3.1 is the TPR - TNR plot, and The below part is the PPV - NPV plot. This geometrical representation is proposed as the confusion plot. The confusion plot in Figure 3.1 is also based on the confusion matrix in Table 2.1. There are four acute angles θ_1, θ_2, θ_3 and θ_4 which are represented as functions of TPR, TNR, PPV and NPV, respectively, such as:

$$\begin{aligned} \cos\theta_1 &= \sqrt{TPR}, \quad \cos\theta_2 = \sqrt{TNR}, \\ \cos\theta_3 &= \sqrt{PPV}, \quad \cos\theta_4 = \sqrt{NPV}. \end{aligned}$$

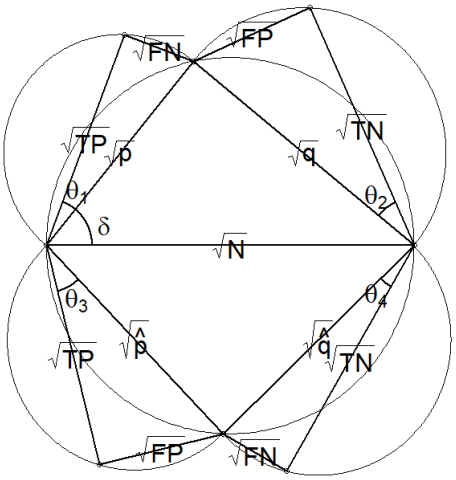

Figure 3.1 Confusion plot

Figure 3.1 tells us that $\theta_1 = 18.4349°$, $\theta_2 = 26.5651°$, $\theta_3 = 30.0000°$, $\theta_4 = 16.1021°$ and $\delta = 50.7685°$. Since θ_1 and θ_4 have smaller values than those of θ_2 and θ_3, respectively, the TPR - TNR plot above is centrally symmetric with the PPV - NPV plot below. We have some examples of confusion matrices and their confusion plots in next section.

4. Illustrative examples

The confusion matrix in Table 2.1 has similar TPR and TNR values as well as FPR and FNR values. Hence the above TPR - TNR plot of Figure 3.1 has an analogous shape with the below PPV - NPV plot. In this section, four kinds of confusion matrices in Table 4.1 are considered. All four tables have $p = 100$ and $q = 125$. The first confusion matrix has large TPR and small TNR values. Second one has small TPR and large TNR. The third has both small TPR and TNR. And last confusion matrix has 1.0 value of both TPR and

TNR, which means perfect classification result. Figure 4.1 contains four different confusion plots corresponding to Table 4.1.

It is found that the angle which means the total probability of disease has $\delta = 48.1897°$ for all four cases in Table 4.1 and Figure 4.1. Since the first confusion plot in Figure 4.1(a) has large TPR and small TNR values, the value of θ_1 has smaller than that of θ_2. And since this has small PPV and large NPV values, the value of θ_3 has larger than that of θ_4. From the second plot in Figure 4.1(b), it has small TPR and large TNR, however both the PPV and NPV have almost equivalent values. Hence θ_1 has larger than θ_2, and both θ_3 and θ_4 have similar values. The third plot in Figure 4.1(c) has the following characteristic: both the TPR and TNR has the same small value, and the PPV is smaller than NPV values, so that both θ_1 and θ_2 have large values, and θ_3 has larger that θ_4. The last plot in Figure 4.1(d) shows that all angles of θ_1, θ_2, θ_3 and θ_4 has zero value, since all value of the TPR, TNR, PPV and NPV is 1.0. Then this confusion plot has a diamond shape. Therefore, one could conclude that a confusion matrix has a close result to perfect classification, when the shape of the confusion plot looks like a rhombus.

Table 4.1 Various confusion matrices

(a)		$\hat{C}$		(b)		$\hat{C}$		(c)		$\hat{C}$		(d)		$\hat{C}$	
		1	0			1	0			1	0			1	0
C	1	90	10	C	1	55	45	C	1	10	90	C	1	100	0
	0	65	60		0	10	115		0	105	20		0	0	125

Table 4.2 Statistics for Table 4.1 and Figure 4.1

	TPR	TNR	PPV	NPV	θ_1	θ_2	θ_3	θ_4
(a)	0.9000	0.4800	0.5806	0.8571	18.4349°	46.1462°	40.3591°	22.2077°
(b)	0.5500	0.9200	0.8462	0.7188	42.1304°	16.4299°	23.0935°	32.0278°
(c)	0.1000	0.1600	0.0870	0.1818	71.5651°	66.4218°	72.8494°	64.7606°
(d)	1.0000	1.0000	1.0000	1.0000	0.0000°	0.0000°	0.0000°	0.0000°

Remark 3 We could derive the following results from the confusion plot:

If TPR > TNR, then $\theta_1 < \theta_2$.
If PPV < NPV, then $\theta_3 > \theta_4$.
If all values of the TPR, TNR, PPV and NPV are large,
then θ_1, θ_2, θ_3 and θ_4 have small values. □

5. Confusion matrices obtained from various normal distributions

The TPR and FNR are defined as $F_1(x)$ and $F_0(x)$ satisfying $F_1(x) \geq F_0(x)$ for $x \in (-\infty, \infty)$, respectivly. Then $F_1(x)$ and $F_0(x)$ are supposed to be two normal distribution functions such as $N(0,\ 1)$ and $N(1,\ \sigma_n^2)$ with $\sigma_n = 0.5, 1.0, 1.5$ and $p = 30, 50, 70$ ($q = 100-p$). For these two distribution functions, thresholds are obtained using the Youden index (Youden, 1950). Based on each threshold, a corresponding confusion matrix is determined. With these confusion matrices, we could draw confusion plots. In particular, when $\sigma_n = 1.0,\ p = q = 50$, all TPR, TNR, PPV and NPV have the same value 0.6915, and $\theta_1 = \cdots = \theta_4 = 33.7402°$. Hence the TPR - TNR plot is symmetrical with the PPV - NPV plot,

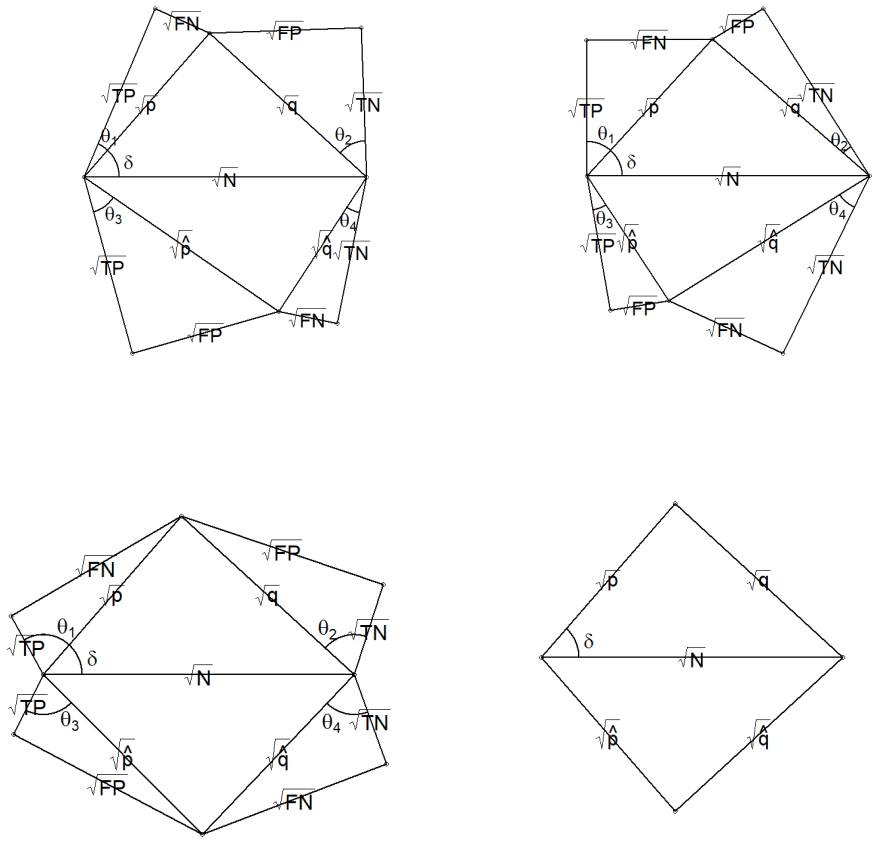

Figure 4.1 Various confusion plots

and the left side of the confusion plot is also symmetrical with the right side. Based on this symmetrical confusion plot, we consider $\sigma_n = 0.5, 1.5$ and $p = 30, 70$ only. The four confusion plots in Figure 5.1 are explored in order to compare.

(Case 1) σ_n is increasing with fixed p and q (compare (a) and (b) or (c) and (d)).

It is found that the TPR increases (TNR decreases), so that θ_1 decreases and θ_2 increases. Also the PPV decreases (NPV increases), so that θ_3 increases and θ_4 decreases. For (a) and (b), the point A1 locates on left side, since $p < q$. On the contrast, for (c) and (d), A1 locates on right side, since $p > q$. Therefore, the point A1 moves to the right, as p increases. Also, the point B1 moves to the right, as $\hat{p}$ increases ($\hat{q}$ decreases). Since the TPR increases, both A2 and A3 points move to the right. Also since the PPV decreases, the point B2 moves to the left and B3 point moves to the right.

(Case 2) p **increases (**q **decreases) with fixed** σ_n (compare (a) and (c) or (b) and (d)).

It is found that both the TPR and TNR are fixed even though the TP increases and the TN decreases, so that both θ_1 and θ_2 are invariant. Nonetheless, the PPV increases (NPV decreases), so that θ_3 increases and θ_4 decreases similarly to Case 1. For (a) and (c) or (b) and (d), both points A1 and B1 move to the right, as both p and $\hat{p}$ are increasing. Since the TPR increases and the PPV increases, A2, A3, B2 and B3 points move to the right.

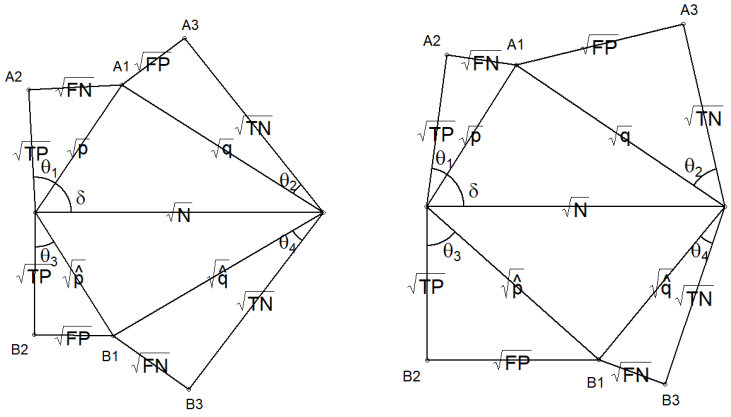

(a) $p = 30, q = 70, \sigma_n = 0.5$ (b) $p = 30, q = 70, \sigma_n = 1.5$

(c) $p = 70, q = 30, \sigma_n = 0.5$ (d) $p = 70, q = 30, \sigma_n = 1.5$

Figure 5.1 Confusion plots for various normal distributions

Table 5.1 Statistics for Figure 5.1

	TPR	TNR	PPV	NPV	θ_1	θ_2	θ_3	θ_4
(a)	0.6485	0.8921	0.7203	0.8555	36.3628°	19.1798°	31.9308°	22.3403°
(b)	0.8167	0.5258	0.4247	0.8700	25.3496°	43.5199°	49.3324°	21.1328°
(c)	0.6485	0.8921	0.9334	0.5210	36.3628°	19.1798°	14.9536°	43.7977°
(d)	0.8167	0.5258	0.8007	0.5514	25.3496°	43.5199°	26.5114°	42.0471°

Remark 4: From the confusion plot, one could derive the following results:
If σ_n is small (the classification result is good), then $\theta_1 > \theta_2$.

If $p > q$, then $\theta_3 < \theta_4$.

Therefore, the comparison of θ_1 and θ_2 depend on the classification results. And the comparison of θ_3 and θ_4 depend on the sample size of p and q. □

6. Empirical data example

Credit evaluation data were collected by a Korean domestic K bank on June 2018. This sample of size 65,455 contains two random variables: one means the RS rank which is a score variable with 20 grades, and the other variable divides each sample into three stages. Hong and Choi (2020) used the second and third stages of size $p = 6,951$ ($C = 1$) and $q = 1,191$ ($C = 0$), respectively. These two stages are classified into non-default and default groups. Hong and Choi (2020) obtained the same 2×2 confusion matrix as in Table 6.1. From Table 6.1, it is obtained that $TPR = sensitivity = 0.9501$, $TNR = specificity = 0.8371$, $PPV = 0.9714$ and $NPV = 0.7418$. All these values are close to 1.0, which means that the accuracy and performance of the diagnosis are superior.

The confusion plot for Table 6.1 is represented in Figure 6.1. From Figure 6.1, we found that both $\theta_1 = 12.9106°$ and $\theta_3 = 9.7257°$ have smaller degrees than $\theta_2 = 23.8031°$ and $\theta_4 = 30.5386°$. Figure 6.1 also tells that $\delta = 22.4864°$, since the total probability of non-default, $p/(p+q)$ has a large ratio 0.8537.

Table 6.1 Confusion Matrix for an empirical data

		$\hat{C}$	
		1/non-default	0/default
C	1/non-default	6604	347
	0/default	194	997

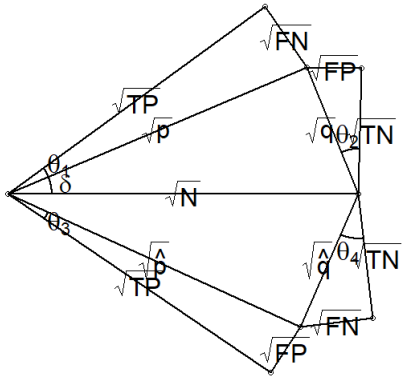

Figure 6.1 Confusion plot

Based on Remark 3 and 4, the confusion plot in Figure 5 tells us the four following findings:

(1) Small values of θ_1 and θ_3 means that the TPR and PPV are large.
(2) Large values of θ_2 and θ_4 means that the TNR and NPV are small.
(3) $\theta_1 < \theta_2$ means that TPR > TNR and the classification result is not good enough.
(4) $\theta_3 < \theta_4$ means that PPV > NPV and $p > q$.

Therefore, we might conclude that the classification results and performance of the empirical data are superior, since values of the TPR and PPV are large enough.

7. Conclusions

The three summation equations in (1) can be obtained from the well known confusion matrix. Three right-angled triangles can be imagined using these three equations. Since these right-angled triangles have common line segments, these triangles can be combined into a single plot, which is called as the TPR - TNR plot. And another three summation equations in (2) are also derived from the confusion matrix. With these three equations, other three right-angled triangles can be drawn. Similarly, these triangles can be put together into one plot, which is suggested as the PPV - NPV plot.

Furthermore, the TPR - TNR and PPV - NPV plots have the same horizontal line segment. And the leftmost and rightmost two line segments of two plots are the same also. Hence, these two plots could be combined into one. The above part is the TPR - TNR plot, and the below part is the PPV - NPV plot. This combined geometrical representation is proposed as the confusion plot.

The four acute angles θ_1, θ_2, θ_3 and θ_4 in the confusion plot could be represented as functions of the TPR, TNR, PPV and NPV, respectively. All these four angles have degrees between 0 to $90°(0,\ \pi/2)$, so that their cosine functions have values between 0 to 1.0. As each angle is decreasing to 0.0, its corresponding ratio increases to 1.0. In conclusion, these acute angles θ_1, θ_2, θ_3 and θ_4 in the confusion plot are represented and explained such as

$$\cos^2\theta_1 \ = \ TPR, \quad \cos^2\theta_2 \ = \ TNR,$$
$$\cos^2\theta_3 \ = \ PPV, \quad \cos^2\theta_4 \ = \ NPV.$$

Also the FPR and FNR can also be described with two angles θ_1 and θ_2 on the confusion plot:

$$\cos^2(\frac{\pi}{2} - \theta_1) \ = \ FNR, \quad \cos^2(\frac{\pi}{2} - \theta_2) \ = \ FPR.$$

Moreover, the total probability of disease, $p/(p+q)$, could be explained with the angle δ satisfying

$$\cos^2\delta \ = \ p/(p+q).$$

Many kinds of confusion matrices which contain various and different FPR and FNR values are considered, From confusion plots corresponding to these confusion matrices, and some features and characteristics are explored and summarized. It is found that this confusion plot can be evaluated the classification model and its performance similarly to the well known ROC curve using comparison values of various angles of right angled triangles. Therefore, the confusion plot proposed in this work could be useful in evaluating the classification models similar to the ROC curve.

References

Altman, D. G. and Bland, J. M. (1994). Diagnostic tests. 1: Sensitivity and specificity. *BMJ: British Medical Journal*, **308**, 1552.

Bamber, D. (1975). The area above the ordinal dominance graph and the area below the receiver operating characteristic graph. *Journal of Mathematical Psychology*, **12**, 387-415.

Centor, R. M. (1991). Signal detectability: The use of ROC curves and their analyses. *Medical Decision making*, **11**, 102-106.

Cho, M. H. and Hong, C. S. (2015). Two optimal threshold criteria for ROC analysis. *The Korean Data & Information Science Society*, **26**, 255-260.

Egan, J. P. and Egan, J. P. (1975). *Signal detection theory and ROC-analysis*, Academic Press.
Engelmann, B., Hayden, E. and Tasche, D. (2003). Testing rating accuracy. *Risk*, **16**, 82-86.
Fawcett, T. (2004). ROC graphs: Notes and practical considerations for researchers. *Machine Learning*, **31**, 1-38.
Fawcett, T. (2006). An introduction to ROC analysis. *Pattern Recognition Letters*, **27**, 861-874.
Green, D. M. and Swets, J. A. (1966). *Signal detection theory and psychophysics (Vol. 1)*, Wiley, New York.
Hanley, J. A. and McNeil, B. J. (1982). The meaning and use of the area under a receiver operating characteristic (ROC) curve. *Radiology*, **143**, 29-36.
Hong, C. S. and Choi, S. Y. (2020). Positive and negative predictive values by the TOC curve. *Communications for Statistical Applications and Methods*, **27**, 211-224.
Hong, C. S. and Joo, J. S. (2010). Optimal thresholds from mixture distributions. *The Korean Journal of Applied Statistics*, **23**, 943-953.
Hong, C. S., Jung, M. S. and Shin, H. S. (2019b). Three-way partial VUS. *Journal of the Korean Data & Information Science Society*, **30**, 445-454.
Hong, C. S., Jung, M. S. and Shin, H. S. (2019a). Partial VUS and optimal thresholds. *Journal of the Korean Data & Information Science Society*, **30**, 895-905.
Hong, C. S. and Lee, S. J. (2018). TROC curve and accuracy measures. *Journal of the Korean Data & Information Science Society*, **29**, 861-872.
Hong, C. S. and Wu, Z. Q. (2014). Alternative accuracy for multiple ROC analysis. *Journal of the Korean Data & Information Science Society*, **25**, 1521-1530.
Hsieh, F. and Turnbull, B. W. (1996). Nonparametric and semiparametric estimation of the receiver operating characteristic curve. *The Annals of Statistics*, **24**, 25-40.
Hughes, G. (2020). On the binormal predictive receiver operating characteristic curve for the joint assessment of positive and negative predictive values. *Entropy*, **22**, 593.
Jeske, D. R. (2018). Metrics used when evaluating the performance of statistical classifiers. *Biostatistics and Biometrics Open Access Journal*, **8**, 7-9.
Metz, C. E. and Kronman, H. B. (1980). Statistical significance tests for binormal ROC curves. *Journal of Mathematical Psychology*, **22**, 218-243.
Oehr, P. and Ecke, T. (2020). Establishment and characterization of an empirical biomarker SS/PV-ROC plot using results of the UBCWkT rapid test in bladder cancer. *Entropy*, **22**, 729.
Pepe, M. S. (2003). *The statistical evaluation of medical tests for classification and prediction*, Medicine.
Pontius Jr, R. G. and Si, K. (2014). The total operating characteristic to measure diagnostic ability for multiple thresholds. *International Journal of Geographical Information Science*, **28**, 570-583.
Provost, F. and Fawcett, T. (1997). Analysis and visualization of classifier performance with nonuniform class and cost distributions. *In Proceedings of AAAI-97 Workshop on AI Approaches to Fraud Detection & Risk Management*, 57-63.
Provost, F. and Fawcett, T. (2001). Robust classification for imprecise environments. *Machine Learning*, **42**, 203-231.
Raslich, M. A., Markert, R. J. and Stutes, S. A. (2007). Selecting and interpreting diagnostic tests. *Biochemia Medica: Biochemia Medica*, **17**, 151-161.
Shiu, S. Y. and Gatsonis, C. (2008). The predictive receiver operating characteristic curve for the joint assessment of the positive and negative predictive values. *Philosophical Transactions of the Royal Society A: Mathematical, Physical and Engineering Sciences*, **366**, 2313-2333.
Sonego, P., Kocsor, A. and Pongor, S. (2008). ROC analysis: Applications to the classification of biological sequences and 3D structures. *Briefings in Bioinformatics*, **9**, 198-209.
Stein, R. M. (2005). The relationship between default prediction and lending profits: Integrating ROC analysis and loan pricing. *Journal of Banking & Finance*, **29**, 1213-1236.
Swets, J. A. (1988). Measuring the accuracy of diagnostic systems. *Science*, **240**, 1285-1293.
Tasche, D. (2008). *Validation of internal rating systems and PD estimates. In the analytics of risk model validation*, Academic Press.
Vuk, M. and Curk, T. (2006). ROC curve, lift chart and calibration plot. *Metodoloski Zvezki*, **3**, 89.
Youden, W. J. (1950). Index for rating diagnostic tests. *Cancer*, **3**, 32-34.
Zhou, X. H., McClish, D. K. and Obuchowski, N. A. (2009). *Statistical methods in diagnostic medicine*, John Wiley & Sons.
Zweig, M. H. and Campbell, G. (1993). Receiver-operating characteristic (ROC) plots: A fundamental evaluation tool in clinical medicine. *Clinical Chemistry*, **39**, 561-577.